Solid-State Electronics Vol. 32, No. 11, pp. 1025–1031, 1989
Printed in Great Britain.

0038-1101/89 $3.00 + 0.00

MODELING OF THE *I–V* CHARACTERISTICS OF SINGLE AND DOUBLE BARRIER TUNNELING DIODES USING A $\mathbf{k}\cdot\mathbf{p}$ BAND MODEL

D. MUI, M. PATIL, J. CHEN, S. AGARWALA, N. S. KUMAR and H. MORKOC
University of Illinois at Urbana-Champaign, Coordinated Science Laboratory, 1101 West Springfield Avenue, IL 61801, U.S.A.

(*Received* 7 *March* 1989; *in revised form* 6 *May* 1989)

Abstract—We model the *I–V* characteristics of single and double barrier tunneling diodes using the complex band structure of the tunneling barrier obtained from a $\mathbf{k}\cdot\mathbf{p}$ band model. Band-bending is calculated by solving two coupled 1-D Poisson's equations with a classical potential in the accumulation region. The transfer matrix method is used for the calculation of the transmission probability of the tunneling electron whose complex **k**-vector is obtained from the band structure. An energy dependent density of states effective mass which is also calculated from the band structure is used. *I–V* characteristics for $In_{0.53}Ga_{0.47}As/In_{0.52}Al_{0.48}As/In_{0.53}Ga_{0.47}As$ single and double barrier tunneling diodes obtained from this model agree quantitatively with experiment.

1. INTRODUCTION

In recent years, a number of novel electronic devices have been proposed whose operational principle is based on quantum mechanical tunneling (QMT). The hot-electron transistor[1–3] and resonant-tunneling diode[4] are examples of such devices. The former device is based on single barrier tunneling while the latter on double barrier tunneling. It is important to have an accurate model to describe QMT because of its importance in modern electronic devices. Due to the inadequacy of the effect mass approximation (EMA) in describing the complex band structure, we have elected to use the $\mathbf{k}\cdot\mathbf{p}$ band model to calculate accurately the electron transmission probability through the barrier. Electronic devices which rely on QMT for their operation have thin tunneling barriers to obtain usable current levels. Due to the presence of a large electric field in these thin barriers, the formation of space charge regions cannot be ignored. It is the purpose of this paper to show that *I–V* characteristics of both single (SBTD) and double (DBTD) barrier tunneling diodes can be modeled accurately when the complex band structure of the barrier and the band-bending in the space charge regions are included in the model. The model for the SBTD is presented first which is then directly extended to the DBTD. Results obtained from this model for both SBTD and DBTD are then compared with experiment.

2. THEORY FOR SBTD

A. Band-bending

Figure 1 shows the conduction band profile of the asymmetrically doped SBTD used in this study under zero bias. Throughout the entire discussion of this paper, we will only be involved with diodes with an undoped tunneling barrier. To avoid dopant diffusion from the terminals into the barrier, which will drastically affect the *I–V* characteristics, undoped $In_{0.53}Ga_{0.47}As$ spacer layers (not shown in the figure, but typically 15 Å thick) are used on both sides of the barrier. In general, band-bending in the space charge regions adjacent to the tunneling barrier is caused by the presence of an electric field in the tunneling barrier. The electric field may be the result of either an external bias or the leveling of the Fermi energy across the whole structure because of asymmetrical doping. For devices where the effect of tunneling is insignificant, which means the smallest dimension of interest is at least a few hundred angstroms, most of the applied bias will appear across the barrier. Consequently, band-bending in the space charge regions are negligible. For the devices under investigation, however, the active layer is of the order of 100 Å thick. A large electric field, therefore, develops across the barrier, even in the presence of only a few hundredths of a volt bias. Due to the continuity of electric displacement across the heterojunction interface, this electric field impresses a space-charge region adjacent to the barrier. To calculate the band-bending in the space charge regions, we need to solve Poisson's equation. When energy is expressed in Rydberg and length in Bohr radius, which are defined by:

$$R_y \equiv \frac{q^4 m_0}{8\epsilon_0^2 h^2} \quad \text{and} \quad a_0 \equiv \frac{\epsilon_0 h^2}{\pi m_0 q^2}$$

respectively, where q is the electronic charge, m_0 is the bare electron mass, ϵ_0 is the absolute dielectric constant, and h is the Planck's constant, the 1-D

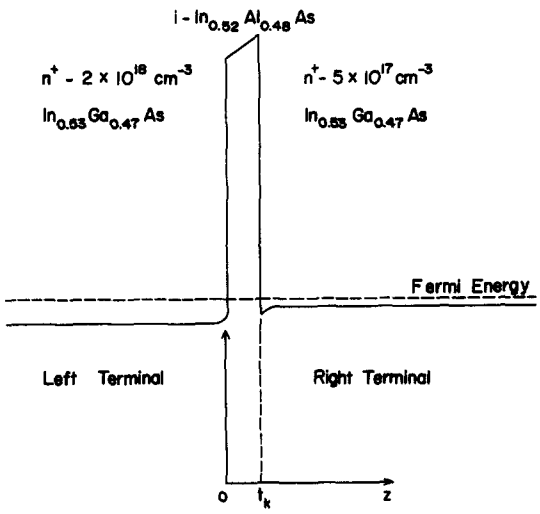

Fig. 1. Conduction band profile of an $In_{0.53}Ga_{0.47}As/In_{0.52}Al_{0.48}As/In_{0.53}Ga_{0.47}As$ single barrier tunneling diode doped to $2 \times 10^{18}\,cm^{-3}$ and $5 \times 10^{17}\,cm^{-3}$ on the left and right terminal, respectively, under zero bias.

Poisson's equation takes the following form[5]:

$$\frac{d^2V(z)}{dz^2} = \frac{8\pi}{\epsilon_1}[n(z) - N], \tag{1}$$

where all the physical quantities are now dimensionless. (Unless otherwise stated, all physical quantities used in this paper are dimensionless.) In the above equation V is the electrostatic potential energy measured relative to the bulk Fermi energy, z is the direction perpendicular to the heterojunction interface, ϵ_1 is the relative dielectric constant of the terminal material, $n(z)$ and N are the electron and dopant densities, respectively. Note that the dopant density is assumed to be uniform and the dopants are assumed to be fully ionized. The latter assumption is justified because our calculation is done for 300 K. Since a high doping density is used, the Fermi–Dirac integral needs to be evaluated exactly with an energy dependent density of states effective mass. (The calculation of this latter quantity is described in the following section.) The quantity $n(z)$ is given by:

$$n(z) = \frac{1}{2\pi^2}\int_0^\infty \frac{m^{*3/2}(E)}{1 + \exp[(E - V(z))/T_R]}\,dE \tag{2}$$

where $m^*(E)$ is the energy dependent density of states effective mass, which is assumed to be isotropic, T_R is the thermal unit defined by $T_R \equiv k_B T/R_y$, with k_B the Boltzmann constant and T the absolute temperature. Two Poisson equations with classical potentials are used in the calculation, one for $z < 0$ and the other for $z > t_k$, where t_k is the thickness of the tunneling barrier (see Fig. 1). The two equations are integrated with respect to the electrostatic potential energy which are then given by:

$$\left(\frac{dV_1(z)}{dz}\right)^2_{z=0} = \frac{16\pi}{\epsilon_1}\left[\int_{V_1(-\infty)}^{V_1(-a)} n(z)\,dV_1 - N_1 \times [V_1(-a) - V_1(-\infty)] + \int_{V_1(-a)}^{V_1(0)} n(z)\,dV_1\right], \quad z < 0, \tag{3a}$$

$$\left(\frac{dV_2(z)}{dz}\right)^2_{z=0} = \frac{16\pi}{\epsilon_1}\left[\int_{V_2(\infty)}^{V_2(a)} n(z)\,dV_2 - N_2 \times [V_2(\alpha) - V_2(\infty)] + \int_{V_2(a)}^{V_2(0)} n(z)\,dV_2\right], \quad z > 0, \tag{3b}$$

where $V_1(-\infty)$ and $V_2(\infty)$ are the Fermi energies of the bulk materials and subscripts 1 and 2 are used for quantities related to the left and right terminal, respectively, and a is the thickness of the undoped spacer layer. Note that we have modeled the spacer and terminal junction as an abrupt junction. We have arbitrarily shifted the z coordinate of eqn (3b) to the left by t_k. The quantities $V_1(0)$ and $V_2(0)$ are then the electrostatic potential energies at the left and right heterojunction interface of the barrier, respectively. The boundary conditions,

$$\left.\frac{dV_1(z)}{dz}\right|_{z=-\infty} = \left.\frac{dV_2(z)}{dz}\right|_{z=\infty} = 0, \tag{4}$$

which state that the electric fields infinitely far from the device are zero, were used in eqns (3). By the condition of continuity of electric displacement across the heterojunction interface, we arrive at:

$$\epsilon_1\frac{dV_1(z)}{dz} = \epsilon_1\frac{dV_2(z)}{dz} = \epsilon_2\frac{V_a + V_2(0) - V_1(0)}{t_k} \tag{5}$$

where V_a is the applied voltage and ϵ_2 is the relative dielectric constant of the tunneling barrier. Equations (2) and (5) are now substituted into eqn (3) which can then be solved as two non-linear algebraic equations. The two quantities $V_1(-a)$ and $V_2(a)$ are not independent variables, they are uniquely determined once $V_1(0)$ and $V_2(0)$ are known. The amount of band-bending in the two space charge regions are obtained by subtracting the Fermi energy of the respective terminal from the electrostatic potential energies $V_1(0)$ and $V_2(0)$. The band-bending on the left and right terminal are symbolized by V_{bl} and V_{br}, respectively. These two quantities and the voltage drop across the tunneling barrier, V_t, are plotted in Fig. 2 for the device shown in Fig. 1 as a function of applied bias. In obtaining Fig. 2, the left terminal of the device is grounded. We have assigned a positive sign to the band-bending for a negative electric field and a negative sign for a positive electric field. Figure 2 shows clearly that the voltage drop across the space charge regions are comparable to that across the tunneling barrier. This suggests that the assumption that all the applied bias appear across the tuneling barrier cannot be used.

B. Tunneling probability

To obtain an accurate figure for tunneling current, the tunneling probability must be calculated

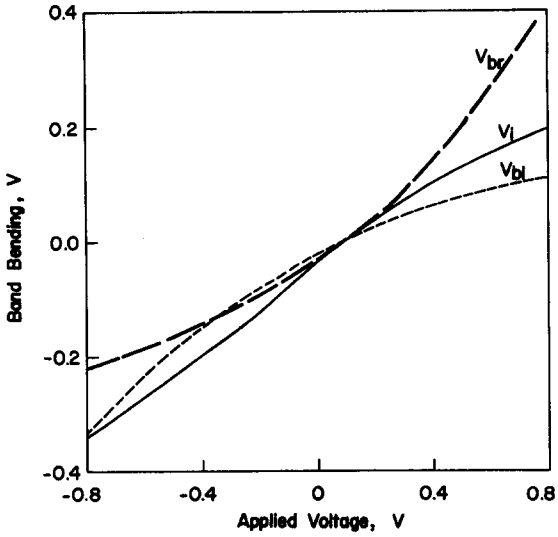

Fig. 2. Band-bending and voltage drop across the single barrier tunneling barrier vs applied bias for the same diode as shown in Fig. 1 with the left terminal grounded.

accurately, The latter depends critically on the complex **k**-vector of the tunneling electron. To calculate the complex **k**-vector, effective mass approximation (EMA) cannot be used because it over estimates this quantity and hence underestimates the current. This comes about because EMA does not take into account the coupling between the conduction and valence bands and, therefore, does not describe the complex band structure properly. There are a number of methods by which the energy band structure can be calculated. These include the $\mathbf{k}\cdot\mathbf{p}$, tight-binding, and pseudopotential methods, to name just a few. All of these methods are rather complicated and involve a considerable amount of computations. Recently, Schuurmans *et al.*[6] proposed a simple 4×4 Hamiltonian based on the $\mathbf{k}\cdot\mathbf{p}$ method and concluded that the model describes properly the complex energy band structure. This method takes into account the coupling of the conduction and the three valence bands exactly, and the effects of higher bands are correct to second-order through a Löwdin renormalization. For the sake of completeness, we repeat this Hamiltonian below:

$$\hat{H}=\begin{bmatrix} E_g+s\hat{E}_z & -\sqrt{\tfrac{2}{3}}iP\hat{k}_z & \sqrt{\tfrac{1}{3}}iP\hat{k}_z & 0 \\ \sqrt{\tfrac{2}{3}}iP\hat{k}_z & -(\gamma_1+2\gamma_2)\hat{E}_z & 2\sqrt{2}\gamma_2\hat{E}_z & 0 \\ -\sqrt{\tfrac{1}{3}}iP\hat{k}_z & 2\sqrt{2}\gamma_2\hat{E}_z & -\Delta-\gamma_1\hat{E}_z & 0 \\ 0 & 0 & 0 & -(\gamma_1-2\gamma_2)\hat{E}_z \end{bmatrix}, \tag{6}$$

Where E_g is the energy gap, Δ is the split-off energy, $\hat{k}_z=-i\partial/\partial z$, $\hat{E}_z=k_z^2/m^*$ (because of the use of dimensionless units, the usual factor of 2 is not present), P is the momentum matrix element, and s, γ_1, and γ_2 describe the coupling of the s and p states to the other bands[6]. The valence band edge is used as the energy reference. Since eqn (6) is a system of equations with constant coefficients, the solutions are linear combinations of exponentials of the form e^{ikz}. We define the energy dependent effective mass $m^*(E_z)$ as

$$m^*(E_z)=\frac{k_z^2}{E_z} \tag{7}$$

With the complex **k**-vector calculated from eqn (6) and the energy dependent effective mass from eqn (7), we can compute the transmission probability by first breaking the tunneling barrier into a series of rectangular steps and then calculate the transfer matrix at each interface. Note that the Hamiltonian given by eqn (6) is basically derived from group theory under zero applied bias. Application of an electric field will break the symmetry and eqn (6) cannot be applied directly. By breaking the barrier into a series of rectangular potential steps, we preserve the symmetry of the original Hamiltonian at each step and eqn (6) can then be used without any modifications.

As explained in Ref. [6], we can assume a separate description of electrons and holes. The boundary conditions then take the following familiar form:

$$\psi(z\to z_r^-)=\psi(z\to z_r^+), \tag{8}$$

$$\left[\frac{1}{m^*(z)}\frac{\mathrm{d}\psi(z)}{\mathrm{d}(z)}\right]_{z\to z_r^-}=\left[\frac{1}{m^*(z)}\frac{\mathrm{d}\psi(z)}{\mathrm{d}z}\right]_{z\to z_r^+}. \tag{9}$$

where z_r is the location of the rth interface and the superscripts + and − indicate z approaches z_r from the right and left, respectively. The transfer matrix at $z=z_r$ is then given by:

$$M_r=\frac{m_R^*}{2k_R}\begin{pmatrix}\alpha_r\exp(-ib_rz_r) & \beta_r\exp(-ia_rz_r)\\ \beta_r\exp(ia_rz_r) & \alpha_r\exp(ib_rz_r)\end{pmatrix}, \tag{10}$$

where $\alpha_r\equiv(k_R/m_R^*)+(k_{R1}/m_{R1}^*)$, $\beta_r\equiv(k_R/m_R^*)-(k_{R1}/m_{R1}^*)$, $a_r\equiv k_R+k_{R1}$, and $b_r\equiv k_R-k_{R1}$, with the subscripts R and R1 relating to quantities of the step to the left and right of the interface at z_r, respectively. The transmission and reflection amplitude, T and R, are thus related by the following product:

$$\begin{bmatrix}1\\ R\end{bmatrix}=\prod_{r=1}^{N}M_r\begin{bmatrix}T\\ 0\end{bmatrix}, \tag{11}$$

where N is the total number of steps taken in the calculation. The incident wave intensity has been normalized to one. Figure 3 shows the situation of the SBTD under positive bias. The formation of the depletion region not only affects the total band-bending picture as discussed earlier but also affects the transmission probability because of the rapid spatial

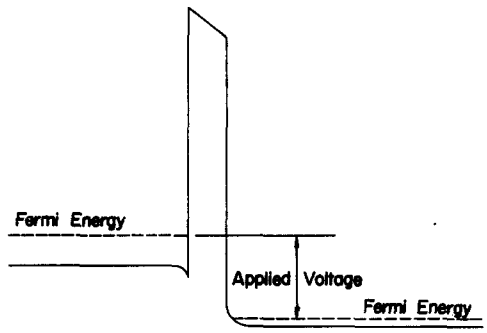

Fig. 3. Conduction band profile of the tunneling diode shown in Fig. 1 under positive bias with the left terminal grounded.

variation of the potential in this region. This latter quantity is calculated by a spatial integration of eqn (1) which is included in the transfer matrices of eqn (11) in obtaining the transmission probability.

The transmission probability as a function of electron energy for electrons tunneling from the left to the right terminal is shown in Fig. 4 for the device shown in Fig. 1 under bias. The conduction band edge of the left terminal is taken to be the energy reference. In the same figure, we have also shown the results of the same calculation using EMA. It should be immediately obvious that EMA gives an underestimation of the transmission probability because of an overestimation of the complex **k**-vector. It is interesting to note that the two curves approach one another at high electron energies (≈ 500 meV). Since the barrier height for this structure is 0.51 eV, at high electron energies the electrons are close to the $In_{0.52}Al_{0.48}As$ band edge where the error in using EMA is the smallest. Consequently, the two curves are close to one another in this energy range. On the other hand, the electrons which contribute most to the current are those lying close to the Fermi energy. Since the Fermi energy is far away from the conduction band edge of the barrier, EMA cannot accurately predict the current density of tunnel diodes.

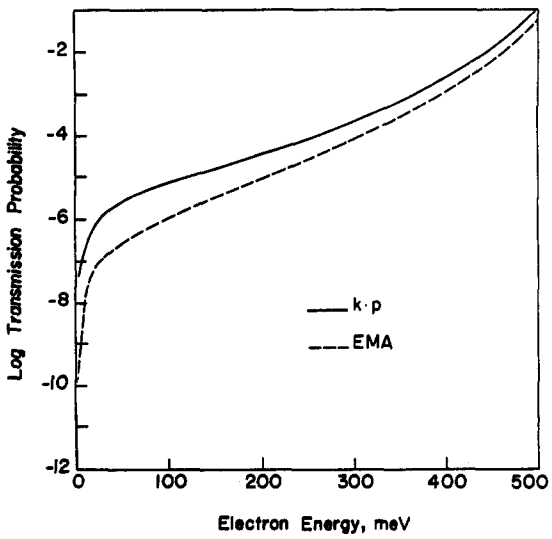

Fig. 4. Comparison of transmission probability obtained from a $\mathbf{k}\cdot\mathbf{p}$ (—) and effective-mass approximation (-----) calculation for the device shown in Fig. 1 under bias.

C. Tunneling current

Instead of using the current density equation derived by Tsu and Esaki[4], we start with the more fundamental equation which relates to the total energy distribution[7]. The forward and reverse tunneling current densities in MKS units are given by

$$j_F = \frac{qm_0}{2\pi^2\hbar^3}\int_0^\infty\int_0^E |T_F(E_z)|^2 \frac{m^{*3/2}(E)}{m^{*1/2}(E_z)} \times\left(\frac{1}{1+\exp[(E-V_1(-\infty)-V_{bl})/K_BT]}\right) +\left(1-\frac{1}{1+\exp[(E-V_2(\infty)+V_{ab}^F)/K_BT]}\right) \times dE_z\,dE, \tag{12a}$$

$$j_R = \frac{qm_0}{2\pi^2\hbar^3}\int_0^\infty\int_0^E |T_R(E_z)|^2 \frac{m^{*3/2}(E)}{m^{*1/2}(E_z)} \times\left(\frac{1}{1+\exp[(E-V_2(\infty)+V_{br})/K_BT]}\right) \times\left(1-\frac{1}{1+\exp[(E-V_1(-\infty)-V_{ab}^R)/K_bT]}\right) \times dE_z\,dE, \tag{12b}$$

where T_F and T_R are the forward and reverse tunneling amplitude, E_z is the energy in the z-direction, $V_{ab}^F \equiv V_i + V_{br}$, and $V_{ab}^R \equiv V_i + V_{bl}$. Note that T_F and T_R are not the same because electrons are assumed to be present at $z = t_k$, i.e., they are not reflected by the depletion region potential, when calculating T_R. To compare this approach with the Tsu and Esaki equation, we have assumed an energy independent effective-mass, the tunneling current densities can be expressed as

$$j_F = \frac{qm_0m^*k_BT}{2\pi^2\hbar^3}\left(\frac{1}{1-\exp[-V_a/k_BT]}\right)\int_0^\infty |T_F(E_z)|^2 \times\left[\ln\left(\frac{1+\exp[(V_1(-\infty)+V_{bl}-E_z)/k_BT]}{1+\exp[(V_2(\infty)-V_{ab}^F-E_z)/k_BT]}\right)\right] \times dE_z, \tag{13a}$$

$$j_R = \frac{qm_0m^*k_BT}{2\pi^2\hbar^3}\left(\frac{1}{1-\exp[V_a/k_BT]}\right)\int_0^\infty |T_R(E_z)|^2 \times\left[\ln\left(\frac{1+\exp[(V_2(\infty)+V_{br}-E_z)/k_BT]}{1+\exp[(V_1(-\infty)+V_{ab}^R-E_z)/k_BT]}\right)\right] \times dE_z, \tag{13b}$$

where V_a is the applied voltage. Despite the similarities of eqns (13) with that given in Ref. [4], there are three major differences. In eqn (13), the effect of band-bending is included, the forward and reverse

tunneling probabilities are calculated explicitly rather than assumed to be the same, and phase-space filling is included for both tunneling currents. Although eqns (12) give the exact current density, nevertheless, it involves a double integration which makes it very time consuming to evaluate. An approximation which relies on the linear dependence of the effective mass with energy is used to reduce it to a single integration while maintaining an energy dependent effective mass. This linear dependence can be expressed as:

$$m(E) = A(E - E_c) + m(E_c) \tag{14}$$

where $m(E_c)$ is the band edge effective mass. The forward current can now be expressed as

$$j_F = \frac{qm_0 k_B T}{2\pi^2 \hbar^3}\left(\frac{1}{1-\exp[-V_a/k_B T]}\right) \times \int_0^\infty T(E_z) I(E_z)\, dE_z, \tag{15}$$

where

$$I(E_z) = Ak_B T[F_1(\eta_1) - F_1(\eta_2)] + [AE_z + m(E_c)]\ln\left(\frac{1+e^{\eta_1}}{1+e^{\eta_2}}\right)$$

with $\eta_1 = (V_1(-\infty) + V_{bi} - E_z)/k_B T$, $\eta_2 = (V_2(\infty) - V_{ab}^F - E_z)/k_B T$, and F_1 is the Fermi–Dirac integral given in Ref. [8] with $j = 1$. A similar expression can be obtained for the reverse current density.

3. THEORY FOR DBTD

Except for the stored charges[9] in the quasi-stationary state in the DBTD, the theory developed above for the SBTD can be directly extended to the DBTD. In the current work we have neglected the stored charges; therefore, the only change that needs to be made in the model for the SBTD is the continuity of electric displacement across the barrier and well. The assumption of no stored charges can be justified as follows. Assume a uniform distribution of charges in the quantum well of the DBTD, the extra voltage drop, V_c, due to these charges is $qCt_w/\epsilon_r\epsilon_0$, where C is the stored charge density, t_w is the well width and ϵ_r is the relative dielectric constant of the well. With an estimated value for C of 10^{11} cm^{-2}[9], V_c is of the order of 10 meV. This is small compared to the peak-current voltage, therefore, the effect of stored charges on the current density should not be important. Since the amount of stored charges depends on the current density, they act as a positive feedback mechanism for the quenching of the resonance peak. This should result in a narrower peak on the I–V curve. We will show that this is in fact the case in the following section.

4. RESULTS AND DISCUSSION

The diodes used in this study are grown by molecular beam epitaxy. The layer structures for the SBTD and DBTD are shown in Figs 5(a) and (b), respectively. Variable size dots ranging from 3 to 100 μm were fabricated on these two structures. Conventional Au–Ge/Ni/Au n-type metallization is used for making electrical contacts. Following the procedure discussed above, we have calculated the tunneling current for these two structures. The most critical parameters used in the calculations are the thickness of the tunneling barrier, the band edge electron and light hole effective masses of $In_{0.53}Al_{0.48}As$, and the conduction band offset. From the calibrated growth rate, the nominal tunneling barrier thickness is 75 Å. Because the tunneling current is sensitive to the tunneling barrier thickness, we have measured the barrier thickness of the SBTD by high resolution transmission electron microscopy (TEM) and obtained a value between 72 and 76 Å. The value of 76 Å is used in the calculation. The layer

(a)

50 Å $n^+ - 5\times10^{18}$ cm^{-3} InAs
0.1 μm $n^+ - 5\times10^{18}$ cm^{-3} $In_{0.53}Ga_{0.47}As$
0.15 μm $n^+ - 2\times10^{18}$ cm^{-3} $In_{0.53}Ga_{0.47}As$
15 Å i–$In_{0.53}Ga_{0.47}As$
76 Å i–$In_{0.52}Al_{0.48}As$
15 Å i–$In_{0.53}Ga_{0.47}As$
0.15 μm $n^+ - 5\times10^{17}$ cm^{-3} $In_{0.53}Ga_{0.47}As$
0.4 μm $n^+ - 5\times10^{18}$ cm^{-3} $In_{0.53}Ga_{0.47}As$
n^+ – InP Substrate

(b)

50 Å $n^+ - 5\times10^{18}$ cm^{-3} InAs
0.1 μm $n^+ - 5\times10^{18}$ cm^{-3} $In_{0.53}Ga_{0.47}As$
0.1 μm $n^+ - 3\times10^{17}$ cm^{-3} $In_{0.53}Ga_{0.47}As$
15 Å i–$In_{0.53}Ga_{0.47}As$
43 Å i–$In_{0.52}Al_{0.48}As$
53 Å i–$In_{0.53}Ga_{0.47}As$
49 Å i–$In_{0.52}Al_{0.48}As$
15 Å i–$In_{0.53}Ga_{0.47}As$
0.125 μm $n^+ - 3\times10^{17}$ cm^{-3} $In_{0.53}Ga_{0.47}As$
0.5 μm $n^+ - 5\times10^{18}$ cm^{-3} $In_{0.53}Ga_{0.47}As$
n^+ – InP Substrate

Fig. 5. Layer structures of the SBTD (a) and DBTD (b) used in this study.

thicknesses which appear in Fig. 5 are the thicknesses used in the calculation. The tunneling current is also sensitive to the electron and light hole effective masses of $In_{0.52}Al_{0.48}As$ but not as sensitive to the momentum matrix element. The electron effective mass by linear interpolation of the values of InAs and AlAs is 0.084. Olego *et al.*[10] reported a value of 0.075 by measuring the electron effective mass at the Fermi energy and then found the band-edge effective mass by correcting for the conduction band non-parabolicity. Furthermore, extrapolation was used to obtain the electron effective mass of $In_{0.52}Al_{0.48}As$. It is difficult to estimate the amount of uncertainty involved in the measurements. A value of 0.084 is used in this work to obtain a good fit to the experimental I–V curve. The value of 0.095 for the light hole effective mass is taken from Ref. [11]. The conduction band discontinuity for this material system is 0.52 eV[12]. Both the theoretical and experimental I–V curves for the single and double barrier diodes are shown in Figs 6(a) and (b), respectively. These curves were obtained with the left terminal grounded. The quantitative agreement between the experimental and theoretical results is reasonably good. Since only the Γ-valley is included in the model, we do not expect the model to be valid for biases where intervalley scattering becomes important. For this material system, this occurs at around 0.55 V, which corresponds to the Γ–L valley separation. The larger discrepency between theory and experiment observed in the DBTD compared to the SBTD is due to the fact that stored charges in the quasi-stationary resonant state are not included in the model. As explained in Section 3, the effect of the stored charges is to make the peak in the I–V curve narrower. This can clearly be seen in Fig. 6(b) by comparing the width of the current peak of the two curves. We should point out that the oscillation observed in the negative differential resistance region in the experimental DBTD I–V curve is not intrinsic to the device and, therefore, the theoretical curve does not show this behavior.

It is interesting to quote the results obtained in a recent paper by Zimmermann *et al.*[13] on the calculation of the I–V characteristics of GaAs/$Al_xGa_{1-x}As$/GaAs SBTD. For the band-bending calculation, they have used both semi-classical and quantum-mechanical methods. The three structures used in their study have nominal tunneling barrier thickness of 180, 300 and 500 Å. They concluded that both methods can be regarded as satisfactory. These results are consistent with our assumption that for very thin tunneling barriers quantum confinement is comparatively less important and a classical potential can be used.

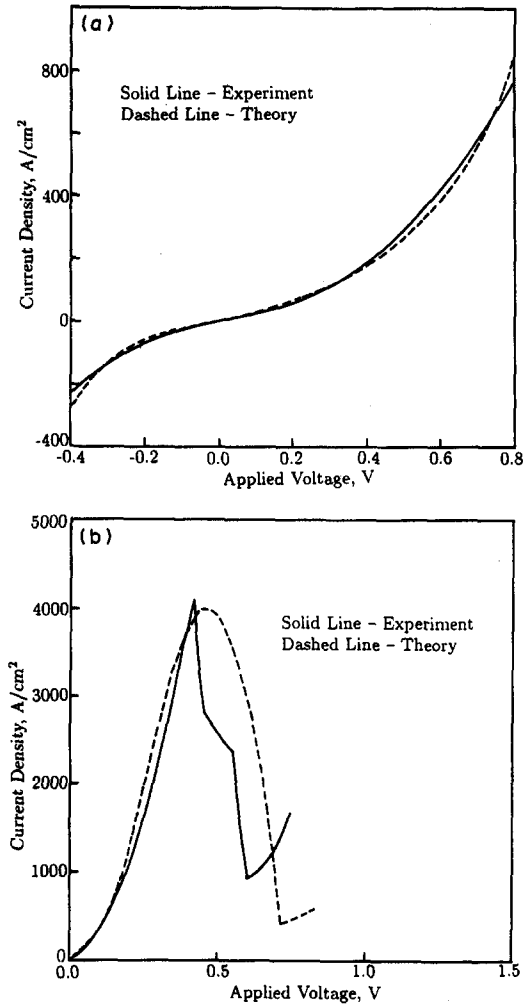

Fig. 6. Theoretical (-----) and experimental (——) I–V curves of the SBTD (a) and DBTD (b).

5. CONCLUSION

We have presented a model for the SBTD and DBTD. Quantitative agreement between theoretical and experimental I–V curves were obtained with this model. We have demonstrated the importance of including band-bending in modeling devices with small geometries. The utility of the transfer matrix method for the calculation of the transmission probability in the $\mathbf{k} \cdot \mathbf{p}$ formalism has been shown. We have also demonstrated the importance of the complex $\mathbf{k}$-vector in the calculation of transmission probability. Since the tunneling current is sensitive to the band edge effective masses of the electron and light hole, confirmation of the accuracy of the calculation presented here can only be done if the effective masses can be measured more accurately. Nevertheless, the use of complex energy band structure in the calculation is an improvement over EMA.

Acknowledgements—This work has been funded by the Air Force Office of Scientific Research and the Innovative Science and Technology Office through the Office of Naval Research under grant # N00014-86-K-0513. One of the authors, D. Mui, would like to acknowledge the IBM

fellowship. The authors would like to thank Dr Chris Kiely for doing the TEM measurements.

REFERENCES

1. J. R. Hayes, A. F. J. Levi and W. Wiegmann, *Phys. Rev. Lett.* **54**, 1570 (1985).
2. M. Heiblum, M. I. Nathan, D. C. Thomas and C. M. Knoedler, *Phys. Rev. Lett.* **55**, 2200 (1985).
3. J. Chen, U. K. Reddy, D. Mui, C. K. Peng and H. Morkoç, *Appl. Phys. Lett.* **51**, 1254 (1987).
4. R. Tsu and L. Esaki, *Appl. Phys. Lett.* **22**, 562 (1973).
5. D. Mui, Master's Thesis, University of Illinois (1987).
6. M. F. H. Schuurmans and G. W. 't Hooft, *Phys. Rev. B* **31**, 8041 (1985).
7. R. D. Young, *Phys. Rev.* **113**, 110 (1959).
8. X. Aymerich-Humet, F. Serra-Mestres and J. Millan, *J. appl. Phys.* **54**, 2850 (1983).
9. V. J. Goldman, D. C. Tsui and J. E. Cunningham, *Phys. Rev. B* **35**, 9387 (1987).
10. D. Olego, T. Y. Chang, E. Silberg, E. Caridi and A. Pinczuk, *Appl. Phys. Lett.* **41**, 476 (1982).
11. W. Stolz, J. C. Maan, M. Altarelli, L. Tapfer and K. Ploog, *Phys. Rev. B* **36**, 4310 (1987).
12. C. K. Peng, A. Ketterson and H. Morkoç, *J. appl. Phys.* **60**, 1709 (1986).
13. B. Zimmermann, E. Marclay and M. Ilegems, *J. appl. Phys.* **64**, 3581 (1988).